07

Optical Band Gap of Pre-Lithiated Si@O@Al Composite

© A.S. Rudy, A.A. Mironenko, V.V. Naumov, S.V. Kurbatov, A.B. Churilov, E.A. Kozlov, O.V. Savenko

Demidov State University, Yaroslavl, Russia
E-mail: rudy@uniyar.ac.ru

Received August 26, 2025
Revised October 14, 2025
Accepted October 22, 2025

The paper presents the results on optical band gap measurements for the Si@O@Al:Li_x anodic composite material, where $x = 0$ at.%; 5 at.% and 9 at.%. Tauc plots were drawn and the optical band gap values were determined based on the absorption spectra of Si@O@Al:Li_x thin films on a quartz substrate. The obtained values were attributed to band-to-band and impurity-to-band transitions. The increase in the optical band gap with increasing x is explained by the Burstein-Moss effect. The calculated energy values of $E_{g1} = 1.52$ eV, $E_{g2} = 1.15$ eV for $x = 0$ at.%, $E_{g1} = 1.93$ eV, $E_{g2} = 1.65$ eV for $x = 5$ at.% and $E_{g1} = 1.85$ eV, $E_{g2} = 1.62$ eV for $x = 9$ at.% were attributed to band-to-band and impurity-to-band transitions, respectively. The optical band gap widening with increasing $x > 0$ is explained by the Burstein-Moss effect.

Keywords: anode material, degenerate semiconductor, band gap, Tauc plot.

DOI: 10.61011/TPL.2026.02.63046.20483

A silicon nanocomposite of the Si@O@Al composition is one of the promising anode materials for thin-film solid-state lithium-ion batteries [1,2]. A composite film is deposited by magnetron sputtering; in standard deposition regimes, its specific capacity is ~ 2500 mA · h/g. One may vary the specific capacity of an anode from 1000 to 3000 mA · h/g by adjusting the target sputtering parameters and the target composition. Unlike nanostructured silicon [3–6], Si@O@Al is highly stable, withstanding more than 1000 charge–discharge cycles without any significant loss of capacity. The main component of Si@O@Al is solid solution a-Si(Al) with small inclusions of nanocrystalline silicon nc-Si(Al), where Si is the solvent and the dissolved component (Al) is indicated in brackets. Since the concentration of the nc-Si(Al) phase is low, it is not mentioned further.

The band structure of a-Si(Al) undergoes significant changes within the charge–discharge cycle of a battery. Subjected to lithiation, degenerate hole semiconductor a-Si(Al) first transforms into a compensated semiconductor, and then into degenerate electron semiconductor a-Si(Al,Li). Accordingly, the resistance of the Si@O@Al composite material undergoes significant changes. This is confirmed by the current–voltage curves (CVCs) in Fig. 1, which correspond to the Ti—Si@O@Al—Ti structure and two Ti—Si@O@Al:Li—Ti structures taken from the center and the edge of a substrate. The spread of CVCs of the Ti—Si@O@Al:Li—Ti structures is attributable to the non-uniformity of magnetron deposition. It can be seen that the film resistance decreases in the process of lithiation, and the Ti—Si@O@Al:Li contact becomes ohmic. The changes in CVCs occurring during lithiation were attributed in [7,8] to compensation of the acceptor impurity (Al) with subsequent formation of the a-Si(Al,Li) degenerate semiconductor phase. The parameters of the Schottky barrier in the Ti—a-Si(Al) contact region were also estimated in these studies. The aim of the present study is to verify the assumptions regarding the existence of two degenerate phases: a-Si(Al) in the delithiated state and a-Si(Al,Li) in the lithiated state. These assumptions may be validated by confirming the presence of band−band and impurity−band electronic transitions in the Si@O@Al absorption spectra.

Thin Si@O@Al films with a thickness of 100 and 200 nm and 100-nm-thick Si@O@Al:Li films were deposited onto

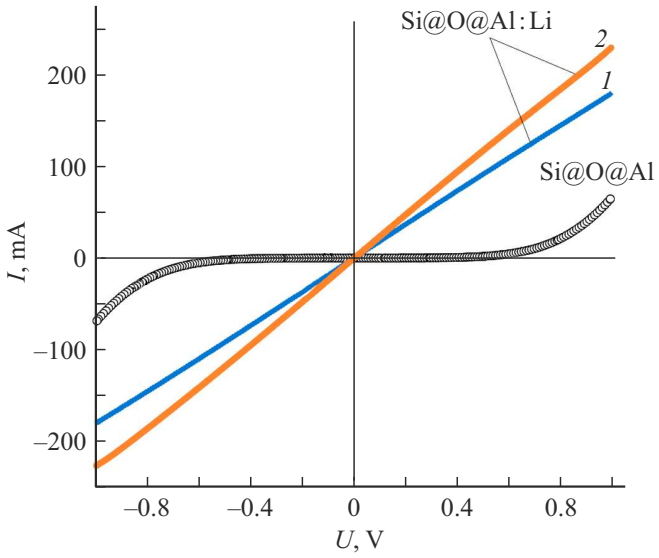

Figure 1. CVCs of test Ti—Si@O@Al—Ti (circles) and Ti—Si@O@Al:Li—Ti (curves *1* and *2*) structures recorded within the range from −1 to +1 V. The spread of characteristics of lithiated samples is attributable to different distances from the center of a substrate (*1* — center; *2* — edge).

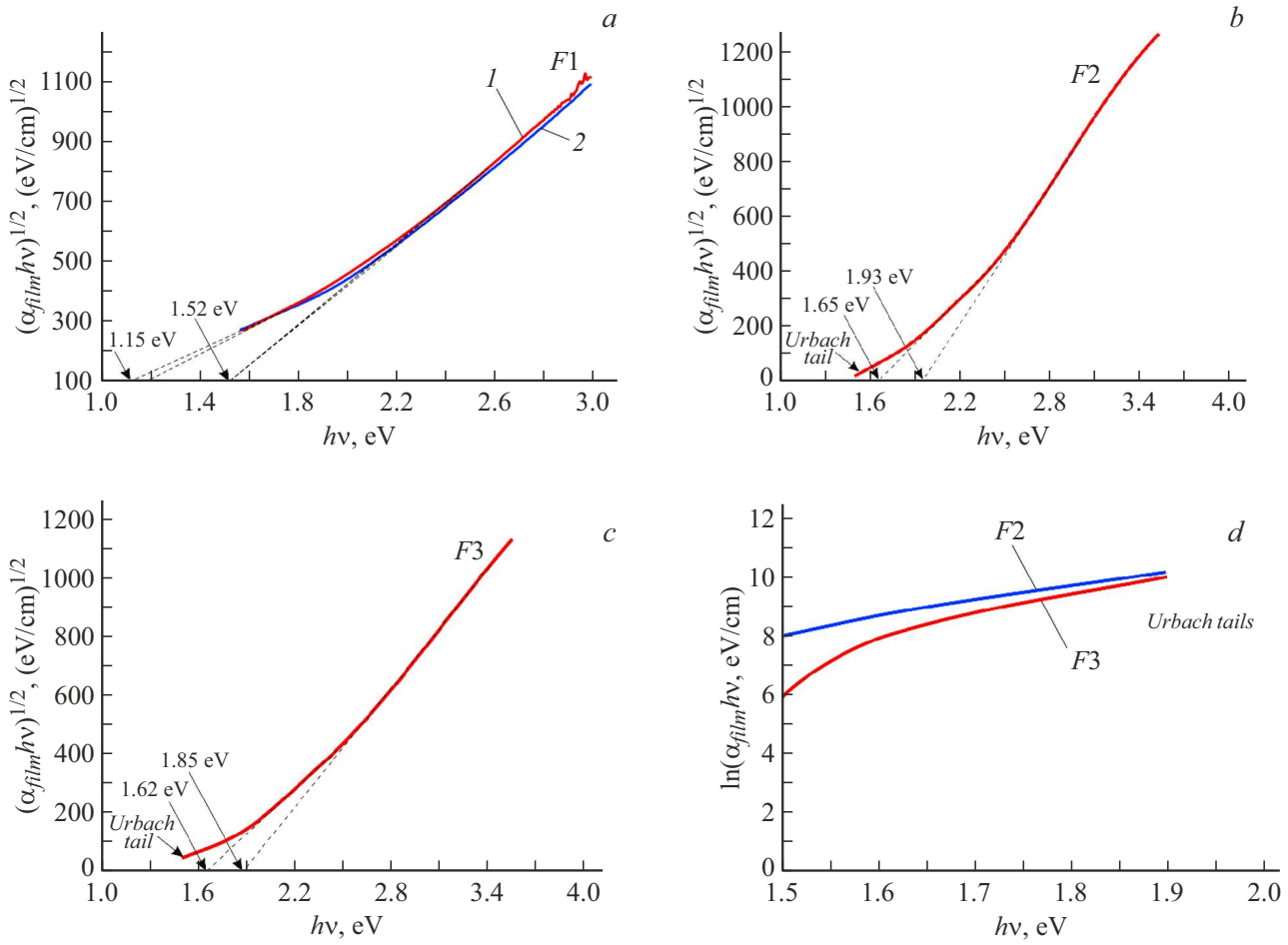

Figure 2. Dependences of $(\alpha_{film}h\nu)^{1/2}$ on $h\nu$ for the determination of E_g by the Tauc method. *a* – Tauc plots for samples $F1$ with a film thickness of 200 (*1*) and 100 nm (*2*) with extrapolation of linear regions; *b* — Tauc plot for sample $F2$; *c* — Tauc plot for sample $F3$; *d* — Urbach tails in the $\ln(\alpha_{film}h\nu)-h\nu$ coordinates.

fused quartz substrates ($D = 40$ mm; thickness, 1.1 mm) by RF magnetron sputtering. Lithium-free films (hereinafter referred to as $F1$) were deposited by sputtering of an Si_3Al target. The films with low ($F2$) and high ($F3$) lithium concentrations were deposited by sputtering $Si_3Al_{0.64} \cdot 0.12Li_2O$ and $Si_3Al_{0.28} \cdot 0.24Li_2O$ targets, respectively. All targets were sputtered under identical conditions in an Ar/O_2 gas mixture. The elemental composition of films was determined by energy-dispersive microanalysis using an EDAX attachment to a Quanta 3D 200i (FEI) microscope. The obtained atomic ratios of elements (lithium excluded) suggest that films $F1$, $F2$, and $F3$ had the compositions of $Si_{66}Al_{20}O_{14}$, $Si_{63}Al_4O_{28}Li_5$, and $Si_{54}Al_3O_{34}Li_9$, respectively.

Absorption spectra were calculated based on the transmission and reflection spectra of the samples, which were measured using an SF-56 (LOMO, Russia) single-channel spectrophotometer within the range of 350–1100 nm. Absorption coefficient α_{film} of the film was calculated as $\alpha_{film} = 4\pi k/\lambda$, where λ is the wavelength of incident light and k is the extinction coefficient of the film under study.

Dependence

$$(\alpha_{film}h\nu)^{1/2} = B(h\nu - E_g), \quad (1)$$

which is known as a Tauc plot [9], was used to determine optical band gap E_g. Here, $h\nu$ is the photon energy corresponding to the wavelength of incident radiation and B is the Tauc parameter. The Tauc parameter is related to the width of tails of the density of localized states of the valence and conduction bands [10,11].

The dependences of $(\alpha_{film}h\nu)^{1/2}$ on $h\nu$ for $F1$, $F2$, and $F3$ layers are shown in Fig. 2. These dependences have two linear sections, which were approximated by linear functions of the form

$$(\alpha_{film}h\nu)^{1/2} = Bh\nu - A. \quad (2)$$

The values of band gap E_g calculated as $E_g = A/B$ are indicated in Figs. 2, *a*–*c*. The Urbach „tail," which is associated with the transitions of electrons from the tail of the density of states of the valence band to the conduction band and from the valence band to the tail of localized states of the conduction band [12], is located in the region of weak

Optical band gap measurement result

Structure	Thickness, nm	Composition	Optical band gap, eV	Transition
$F1$	200 100	$Si_{66}Al_{20}O_{14}$	1.19 1.52 1.15 1.52	Impurity−band Band−band Impurity−band Band−band
$F2$	100	$Si_{63}Al_4O_{28}Li_5$	1.65 1.93	Impurity−band Band−band
$F3$	100	$Si_{54}Al_3O_{34}Li_9$	1.62 1.85	Impurity−band Band−band

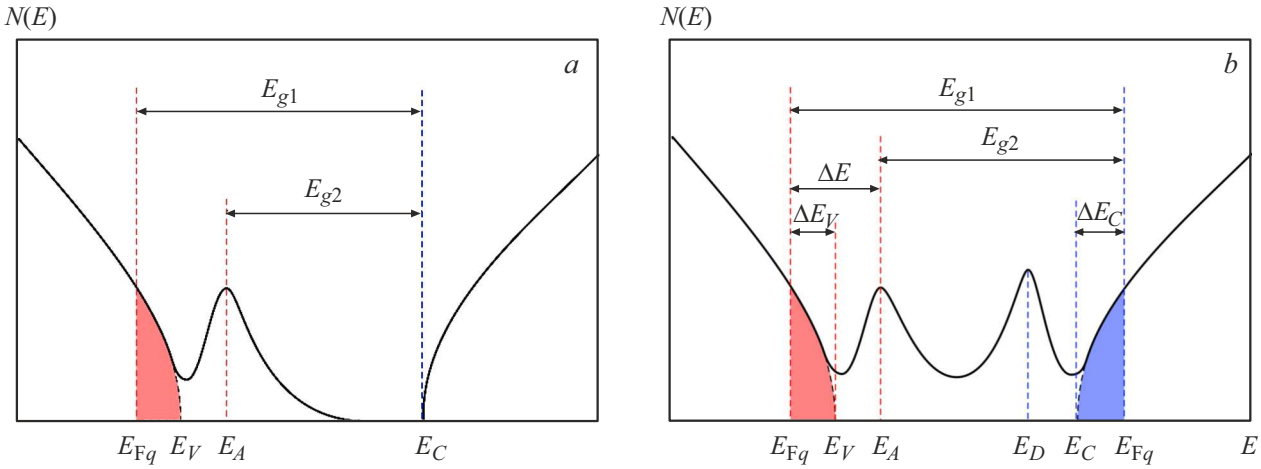

Figure 3. Approximate form of the density of electronic states in solid solutions a-Si(Al) and a-Si(Al,Li). a — Formation of an impurity band in degenerate a-Si(Al) (transitions corresponding to E_g in Fig. 2, a are shown). b — Impurity bands in a-Si(Al,Li) (possible band−band and impurity−band transitions in a nonequilibrium system and an increase in optical band gap $\Delta E_{\mathrm{BM}} = \Delta E_V + \Delta E_C$ due to the Burstein−Moss effect are indicated).

absorption ($\alpha_{film} < 10^4\,\mathrm{cm}^{-1}$, $h\nu < 1.87\,\mathrm{eV}$). According to theory [12], the absorption coefficient in the region of this Urbach tail depends on photon energy in the following way:

$$\alpha_{film} \propto \frac{\exp(h\nu/E_0)}{h\nu}, \qquad (3)$$

where E_0 is the Urbach energy. Figure 2, d shows the dependences of $\ln(\alpha_{film} h\nu)$ on $h\nu$ for samples $F2$ and $F3$. These dependences are linear (the $F3$ dependence is linear within the 1.6−1.87 eV interval), which is consistent with formula (3). The optical band gap measurement results are listed in the table.

According to the current understanding of the energy structure of a degenerate semiconductor [13], the intrinsic and impurity bands merge at impurity concentration $n_{imp} > r_{\mathrm{B}}^{-3}$, where r_{B} is the Bohr radius of the impurity in the semiconductor. The density of states function of the a-Si(Al) phase, which forms the basis of Si@O@Al, should then take the form shown schematically in Fig. 3, a. With subsequent lithiation of a-Si(Al), the acceptor impurity is compensated, and the donor impurity band then merges with the conduction band of silicon. The corresponding density of states functions are shown schematically in Fig. 3, b.

Two types of transitions are possible in a semiconductor of this kind: band−band and impurity−band ones. These transitions yield two values of the optical band gap: E_{g1} (band–band transition) and E_{g2} (impurity–band transition). Since the a-Si(Al,Li) phase is a semiconductor heavily doped with acceptor and donor impurities, the Burstein–Moss effect [14] may be associated with a shift of the Fermi level in both valence and conduction bands. One may then introduce two quasi-Fermi levels $E_{\mathrm{F}q}$: one for the valence band and one for the conduction band (see Fig. 3, b). If the system is close to equilibrium, all states in the valence band are filled and $\Delta E_V = 0$.

Thus, the absorption spectra of structures $F1$, $F2$, and $F3$ with different lithium concentrations provide a more detailed insight into the band structure changes in

individual phases of Si@O@Al in the process of lithiation (specifically, during the a-Si(Al)→ a-Si(Al,Li) transition). Tauc plots are indicative of the existence of two transitions (band−band and impurity−band) in the a-Si(Al,Li) phase. This implies that two impurity bands (acceptor and donor) are formed. The magnitude of the Burstein−Moss shift is large, suggesting a strong a-Si(Al,Li) degeneracy.

Funding

This study was supported financially by the Ministry of Science and Higher Education of the Russian Federation under state assignment FENZ-2024-0005 for the Demidov Yaroslavl State University.

Conflict of interest

The authors declare that they have no conflict of interest.

References

[1] T.L. Kulova, A.A. Mironenko, A.M. Skundin, A.S. Rudy, V.V Naumov, D.E. Pukhov, Int. J. Electrochem. Sci., **11** (2), 1370 (2016). DOI: 10.1016/S1452-3981(23)15928-1
[2] A.A. Mironenko, I.S. Fedorov, A.S. Rudy, V.N. Andreev, D.Y. Gryzlov, T.L. Kulova, A.M. Skundin, Monatsh. Chem., **150** (10), 1753 (2019). DOI: 10.1007/s00706-019-02497-1
[3] A.P. Nugroho, N.H. Hawari, B. Prakoso, A.D. Refino, N. Yulianto, F. Iskandar, E. Kartini, E. Peiner, H.S. Wasisto, A. Sumboja, Nanomaterials, **11** (11), 3137 (2021). DOI: 10.3390/nano11113137
[4] A.D. Refino, N. Yulianto, I. Syamsu, A.P. Nugroho, N.H. Hawari, A. Syring, E. Kartini, F. Iskandar, T. Voss, A. Sumboja, E. Peiner, H.S. Wasisto, Sci. Rep., **11** (1), 19779 (2021). DOI: 10.1038/s41598-021-99173-4
[5] H. Li, Z. Wang, L. Chen, X. Huang, Adv. Mater., **21** (45), 4593 (2009). DOI: 10.1002/adma.200901710
[6] H. Li, H. Li, Y. Lai, Z. Yang, Q. Yang, Y. Liu, Z. Zheng, Y. Liu, Y. Sun, B. Zhong, Z. Wu, X. Guo, Adv. Energy Mater., **12** (7), 2102181 (2022). DOI: 10.1002/aenm.202102181
[7] A.S. Rudy, A.B. Churilov, A.A. Mironrenko, V.V. Naumov, S.V. Kurbatov, E.A. Kozlov, Tech. Phys. Lett., **48** (9), 7 (2022). DOI: 10.21883/TPL.2022.09.55072.19276.
[8] A.S. Rudy, A.A. Mironenko, V.V. Naumov, A.B. Churilov, S.V. Kurbatov, Yu.S. Egorova, E.A. Kozlov, Tech. Phys., **68** (9), 1235 (2023). DOI: 10.21883/JTF.2023.09.56220.120-23 [A.S. Rudy, A.A. Mironenko, V.V. Naumov, A.B. Churilov, S.V. Kurbatov, Yu.S. Egorova, E.A. Kozlov, Tech. Phys., **68** (9), 1235 (2023). DOI: 10.61011/TP.2023.09.57363.120-23].
[9] J. Tauc, R. Grigorovici, A. Vancu, Phys. Status Solidi B, **15** (2), 627 (1966). DOI: 10.1002/pssb.19660150224
[10] F.L. Martínez, M. Toledano-Luque, J.J. Gandía, J. Cárabe, W. Bohne, J. Röhrich, E. Strub, I. Mártil, J. Phys. D, **40** (17), 5256 (2007). DOI: 10.1088/0022-3727/40/17/037
[11] F.L. Martínez, A. Prado, I. Mártil, G. González-Díaz, B. Selle, I. Sieber, J. Appl. Phys., **86** (4), 2055 (1999). DOI: 10.1063/1.371008
[12] *Amorphous and liquid semiconductors*, ed. by J. Tauc (Springer, 2012).
[13] P.K. Kashkarov, V.Yu. Timoshenko, *Optika tverdogo tela i sistem ponizhennoi razmernosti* (Fiz. Fak. Mosk. Gos. Univ., M., 2009) (in Russian).
[14] T. Moss, Proc. Phys. Soc. B, **67** (10), 775 (1954). DOI: 10.1088/0370-1301/67/10/306

Translated by D.Safin